Materials Research. 2022; 25:e20210315
DOI: https://doi.org/10.1590/1980-5373-MR-2021-0315

Development of a β-$LiAlSi_2O_6$:Cr-based Ceramic Pigment by Proteic Sol-Gel Process Using Gelatin: Synthesis and Characterization

Ricardo Ferrari Ferraz[a]*, Jaine Ferreira Sousa[a], Daniel dos Santos Costa[a], Raquel Aline Pessoa Oliveira[a], Héstia Raissa Batista Reis Lima[b]

[a]Universidade Federal do Vale do São Francisco, 48920-310, Juazeiro, BA, Brasil.
[b]Instituto Federal de Sergipe, 49400-000, Lagarto, SE, Brasil.

Received: June 28, 2021; Revised: October 08, 2021; Accepted: October 25, 2021

A novel pigment of β-$LiAlSi_2O_6$:Cr ceramic was developed by a partial proteic sol-gel process, using gelatin as a ligand. X-ray diffraction (XRD), energy dispersive spectroscopy (EDS) and visible and near-infrared diffuse reflectance spectroscopy (vis-NIR DRS) were performed. XRD results confirmed that the crystal structure of the lattice corresponded to β-$LiAlSi_2O_6$ (or β-spodumene), and the addition Cr^{3+} ions by doping did not interfere in the formation of this crystalline phase. EDS confirmed the homogeneous existence of Cr^{3+} dopant in β-$LiAlSi_2O_6$ particles. From the vis-NIR DRS, selective absorption of visible light wavelengths was identified in the bands of 425 nm and 600 nm, resulting in the perception of a yellowish-green color when β-$LiAlSi_2O_6$ is doped with Cr^{3+}. CIE-XYZ colorimetric coordinates were generated to characterize the resulting colors. The obtained results demonstrated the viability of β-$LiAlSi_2O_6$:Cr synthesis by a proteic sol-gel route and its great potential for obtaining a yellowish-green ceramic pigment.

Keywords: *proteic sol-gel process, gelatin, β-spodumene, ceramic pigment.*

1. Introduction

Ceramic pigments can assign color from the dispersion of insoluble particles. The selective absorption of visible light wavelengths occurs due to the action of a chromophore ion (usually transition metals) incorporated in the structure of the lattice[1]. The chromophore ions whose radius and charge properties are close to the ions replaced can be introduced in the crystalline structure by high temperature synthesis[2]. Pigments can assign different color possibilities to the materials, depending on the addition of the dopant, the quantity, the type, and the method of production[3]. These colors are responsible for technological applications that are quite vast, encompassing both the cosmetics and dental materials industries, as well as paints, resins, plastics, among others[4]. In some cases, mechanochemical using ball milling or other processing techniques can be applied to pigment powders to form nanopowders, increasing specific surface area and improving their performance[5].

The production of pigments based on the structure of silicates and aluminosilicates as novel raw material alternatives has increased significantly[6-9], mainly due to its high availability, in contrast to others scarce materials. Among the materials capable of forming ceramic pigments is $LiAlSi_2O_6$ (spodumene), which is a mineral of importance in the extraction of lithium and has also been obtained synthetically for several applications[10-15]. Spodumene, in its natural polymorphic form of hiddenite, has a greenish color due to the presence of Cr^{3+} in its matrix, which is shown to be mostly in Al^{3+} sites[16] and probably occurs due to the similarity of the properties of the ions (radius and charge). Moreover, this pyroxene mineral has thermal stability and is chemically inert. However, the synthesis of $LiAlSi_2O_6$-based pigments, after extensive bibliographic research, has not been reported.

Several methods can be used for the oxide pigments synthesis, the most common being the solid-state reaction, based on the ionic diffusion process. However, the high temperatures used and problems with homogenization are disadvantages of this method[17]. Therefore, solution chemical synthesis techniques are preferably employed to reduce synthesis temperatures and produce materials with good homogeneity, such as sol-gel, Pechini[18], combustion method, among others. The advantage of combustion method is enabling it to synthesize pigments in short reaction times and at a moderate temperature, however, the process is uncontrollable[19]. The Pechini method provides homogeneous powders with small particle size, high purity and relatively low calcination temperatures[20]. However, most of them employ environmentally hazardous reagents or highly complex processes involved in the synthesis that may limit its application on an industrial scale[21].

The sol-gel route represents a valuable technique for obtaining materials, in which the organic and inorganic members are closely linked[22,23], and shows a few advantages, including the ability to produce a solid-phase material from a chemically homogeneous precursor[24]. This method is used in several applications, mainly due to the good homogeneity and low sintering temperatures[10]. In a proteic sol-gel method[25],

*e-mail: ricardo.univasf@gmail.com

the precursor metal alkoxides are replaced by proteic ligands. Coconut water was initially used, and gelatin powder is commonly used due to its high concentrations of partially hydrolyzed collagen[26]. This organic ligand is from a renewable source, being considered an eco-friendly reagent[27]. The gel is produced by the partial hydrolysis of peptide bonds and a consecutive formation of cross-links in the gelation process[28]. The precursor metals (and semimetals) can be included as soluble salts in the colloidal solution. For this method, the heating rates for the drying and calcining processes must be slow enough to prevent material retraction during solvent elimination and organic cross-linked polymeric chains degradation.

In this context, this paper reports the development of β-$LiAlSi_2O_6$, which corresponds to the synthetic polymorph of spodumene with a tetragonal structure, doped with Cr^{3+} ions and synthesized by a proteic sol-gel route using gelatin as a ligand, aiming at the production of a novel ceramic pigment. The processes of synthesis and characterization of the crystalline structure and optical behavior are discussed.

2. Experimental

The production of the material was based on the methodological procedure described by Lima et al.[10], who established a proteic sol-gel route for the synthesis of pure β-$LiAlSi_2O_6$ using silica precursor. The authors identified, from thermal analyzes (TGA and DTA), that the total decomposition of the polymer chains and the beginning of the formation of the β-$LiAlSi_2O_6$ crystalline phase occurred at a temperature of 700 ºC, but the complete formation of the single-phase occurred over 1000 °C.

A solution containing a 1:2 ratio of gelatin:reagents was initially prepared. For this solution, the stoichiometric proportions were obeyed by the balanced chemical reaction (Equation 1) containing the reagents of basic composition for the formation of 1 g of β-$LiAlSi_2O_6$. This route can be considered as a hybrid of sol-gel and solid-state reactions since silica is insoluble in the initial solution. In this way, it is treated in this paper as a partial proteic sol-gel route.

$$\begin{aligned} &LiNO_3 + Al(NO_3)_3.9H_2O + 2SiO_2 \xrightarrow{T=1100\,^{\circ}C} \\ &\beta - LiAlSi_2O_6 + 4HNO_3(gas) + 7H_2O(gas) \end{aligned} \quad (1)$$

Initially, 20 mL of distilled water were heated to 70 ºC and were added: 20 mL of $LiNO_3$ (Dinâmica®, purity of 95%) solution (0.27 mol/L), 20 mL of $Al(NO_3)_3.9H_2O$ (Dinâmica®, purity of 98.5%) solution (0.27 mol/L) and 0.646 g of SiO_2 (NEON, purity of 98%) powder. Samples were produced containing weight percentages of Cr_2O_3 (NEON, purity of 98%) – 0.5, 1, 1.5, 2, 2.5, and 3%. As a ligand, 1.516 g of gelatin powder (Royal®) dissolved in 20 mL of distilled water was added. The final solutions were heated to 200 ºC with constant magnetic stirring for 1 h to the gels forming. The gels obtained were submitted to oven drying at 100 ºC for 48 h to form the xerogels.

After drying, the xerogels were macerated with a porcelain mortar and taken to precalcination in a resistive oven at 700 ºC for 2 h at a heating rate of 10 ºC/min in an alumina crucible (boat), for the decomposition of nitrates and loss of organic ligands (pyrolysis of gelatin), followed by slow cooling, in closed oven. Samples were removed at room temperature (25 ºC). After a second maceration, under the same conditions, all samples were calcined in a resistive oven at 1100 ºC for 2 h at a heating rate of 10 ºC/min in the alumina crucible, for the formation of the crystalline structure of β-$LiAlSi_2O_6$. The final samples were removed at room temperature (25 ºC) after slow cooling. The samples were macerated one last time and sieved to obtain suitable granulometry for X-ray diffraction (75 - 150 μm) and vis-NIR diffuse reflectance electronic spectroscopy (< 75 μm).

X-ray diffraction (XRD) measurements were taken with a powder diffractometer Rigaku Miniflex, with Cu-K_α radiation (λ = 1.5418 Å), with the tube operating at 40 kV/15 mA in the continuous mode with steps of 0.02 º, speed of 10 º/min and room temperature. The experimental results obtained were compared with the theoretical patterns available in the PDF2 (Powder Diffraction File) crystallographic database from the positions and intensities of the Bragg crystalline peaks and the most likely references selected using the software X'Pert HighScore Plus (PANalytical B. V.). The Rietveld refinement method[29] was provided to ratify the occurrence of the β-$LiAlSi_2O_6$ phase for the samples produced, using the DBWSTools 2.4 program[30].

Energy dispersive spectroscopy (EDS) analysis was taken with a scanning electron microscope (SEM) Vega 3XM (Tescan) at accelerating voltage of 20 kV equipped with an EDS detector. The powdered samples were placed on carbon strips and submitted to the metallization process with a thin layer of gold, in order to improve the quality of the analyzed micrographs, due to the better electrical conductivity provided. The analysis of elements present in sample particles was performed by SEM image and overlaid EDS at 1000x magnification.

The vis-NIR diffuse reflectance electronic spectroscopy (vis-NIR DRS) measurements were performed in a spectrometer FieldSpec®3 (Analytical Spectral Devices) with optical sensor with 8 ° field vision, operating with wavelengths ranging from 400 nm to 2000 nm, resolution from 3 to 10 nm and scanning time of 100 ms, a 50 W quartz and tungsten halogen light source, a darkroom measuring 100 x 50 x 50 cm, and a computer with RS3 software (Analytical Spectral Devices). A ceramic plate Spectralon® (Labsphere Inc.) was used as white standard reference. Spectra were provided in absorbance values and converted into colorimetric coordinates of the CIE-XYZ[31] space using the SpectraLux 1.0 software (Ponto Quântico Nanodispositivos).

3. Results and Discussions

X-ray powder diffractograms obtained for β-$LiAlSi_2O_6$ samples, calcined at a temperature of 1100 ºC, doped with different concentrations of Cr^{3+}, are plotted in Figure 1. The experimental XRD patterns were compared with the standard reference ICSD 26817, corresponding to β-$LiAlSi_2O_6$ with a tetragonal crystalline structure[32]. All samples have identical crystalline structures and their peaks are well defined. When comparing the experimental XRD patterns with the standard reference ICSD 26817, the positions and intensities of the peaks are corresponding, demonstrating the success of the

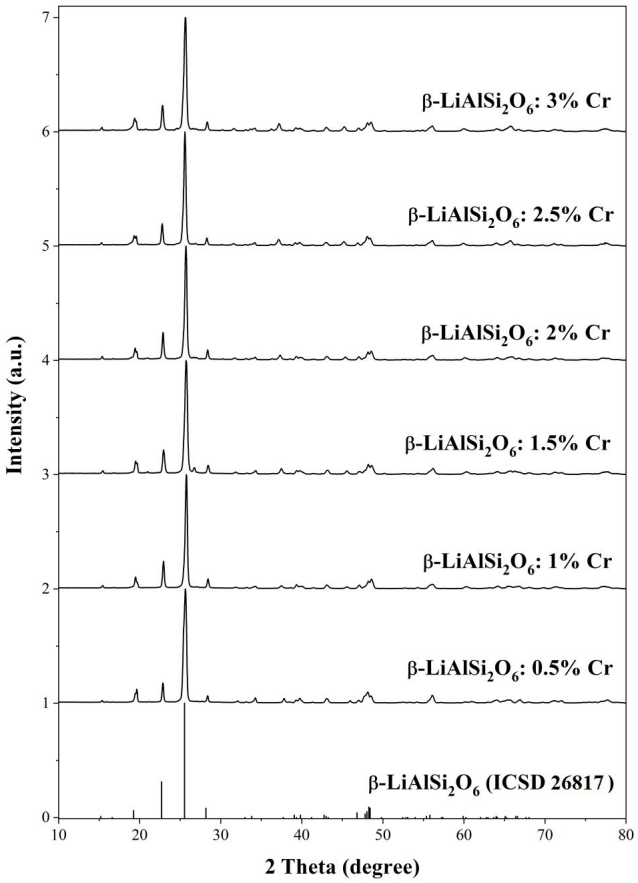

Figure 1. Experimental XRD patterns of β-$LiAlSi_2O_6$:Cr and the standard reference ICSD 26817.

synthesis. The presence of the dopant in the material did not cause distortions in the crystalline lattice, which is possibly due to the insertion of Cr^{3+} ions to vacancies of Al^{3+}, since the chemical properties (charge and radius) are close.

Figure 2 presents the experimental X-ray powder diffraction (XRPD) patterns, the XRD calculated by the Rietveld method and the intensities difference for the samples of β-$LiAlSi_2O_6$:Cr. The XRD patterns were compared with the standard reference ICSD 26817, being verified that the used sample corresponds to β-$LiAlSi_2O_6$, which belongs to the tetragonal crystal system having the space group P43212. The crystallographic parameters are: a = b = 7.5410 Å, c = 9.1560 Å, α = β = γ = 90º; density = 2.37 g/cm^3; and volume = 520.67 x 10^6 pm^3.

The results of the Rietveld refinement obtained from the analysis are expressed as index indicating disagreement, in percentage. This index is as values of permitted error (R_P), obtained error (R_{WP}), expected error (R_E), and the ratio R_{WP}/R_E (or, simply, χ)[33]. The χ value is of critical importance, as long as χ = 1 means that the calculated spectrum is perfectly adjusted to the experimental spectrum[34]. Factors close to the unit indicate a good fit, since the errors obtained in the process (R_{wp}) are close to the expected errors (R_e)[35]. Bragg R-factor (R_{Bragg}) is quoted as an indicator of the quality of the fit between observed and calculated[36] and the values obtained demonstrate that the 0.5 to 2.5% Cr^{3+}-doped samples approximate 12 to 16% of the crystalline structure of a perfect β-$LiAlSi_2O_6$ crystal. For the β-$LiAlSi_2O_6$:3%Cr sample, an increase in the 'χ factor' to 1.90 and in the Bragg R-factor to 22.6% was identified, indicating that possibly the increase in Cr^{3+} content over 3.0% may start a dopant saturation point. Despite this, no additional phases were identified by the refinement. All refinement factors, in detail, are shown in Table 1.

SEM image and overlaid EDS for the β-$LiAlSi_2O_6$:3%Cr sample is shown in Figure 3. In Figure 3a, a particle with an average diameter of 150 μm is emphasize, and has an irregular and angular shape. This type of particle morphology has already been verified for β-$LiAlSi_2O_6$[37]. Lithium locations are not possible to be detected by the equipment, due to its low energy of characteristic radiation. Figure 3b-e illustrated the element mapping of Si, Al, Cr and O. It is clearly perceived that the Cr^{3+} distribution had similar contours to the particle in Figure 3a, verifying the homogeneous existence of Cr^{3+} dopant in β-$LiAlSi_2O_6$ particles. This was conceivable because the supply of precursors and dopant by the proteic sol-gel method undergoes in an aqueous solution, which can easily blend all components uniformly. A similarity between the contours for the dopant Cr^{3+} and the elements Al and Si is noticed. The great possibility of Cr^{3+} occupying Al^{3+}

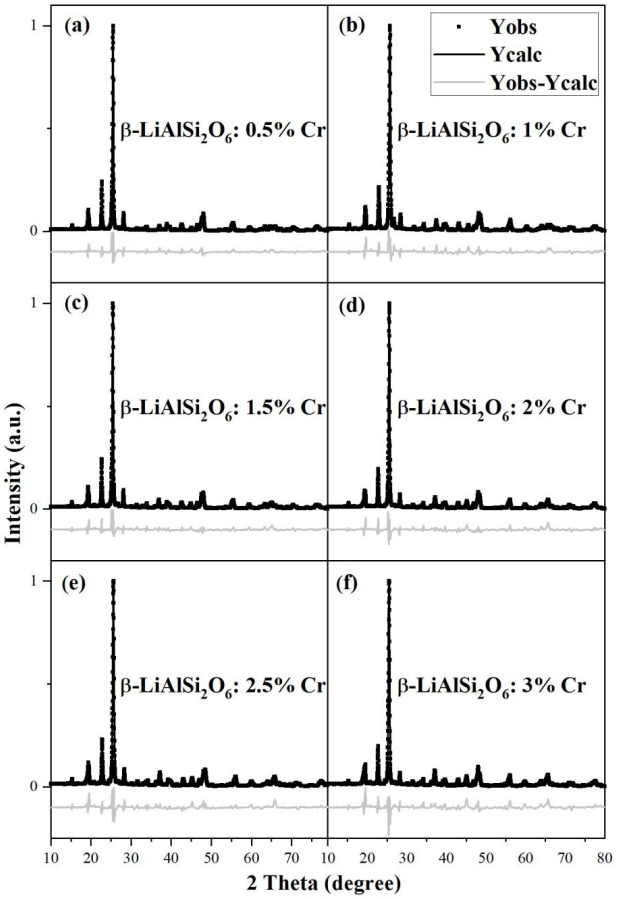

Figure 2. Y(obs) X-ray diffraction pattern for different samples of β-$LiAlSi_2O_6$:Cr and Y(calc) spectra calculated by Rietveld method. The result of refinement is the difference Y(obs) - Y(calc).

Table 1. Quality factors of the Rietveld refinement for β-$LiAlSi_2O_6$:Cr samples.

Sample	R_p (%)	R_{wp} (%)	R_e (%)	χ	R_{Bragg} (%)
β-$LiAlSi_2O_6$:0.5%Cr	14,47	19,23	12,92	1,48	12,07
β-$LiAlSi_2O_6$:1%Cr	15,68	21,47	12,98	1,65	11,95
β-$LiAlSi_2O_6$:1.5%Cr	14,40	19,12	13,08	1,45	11,71
β-$LiAlSi_2O_6$:2%Cr	16,90	22,82	13,35	1,70	13,96
β-$LiAlSi_2O_6$:2.5%Cr	15,64	21,07	13,47	1,56	15,97
β-$LiAlSi_2O_6$:3%Cr	19,77	26,00	13,64	1,90	22,61

sites in the structure of natural spodumene has already been observed[16], however, for β-$LiAlSi_2O_6$, the Si^{4+} ions and Al^{3+} share the same occupation site, and it is very possible that Cr^{3+} occupy these sites when added as a dopant. This occurs considering Al^{3+} and Cr^{3+} equal charges and coordination numbers, as well as their similar ionic sizes.

The spectra from the vis-NIR DRS, converted in absorbance values for the samples produced, are plotted in Figure 4. Four main spectral signatures have been identified, corresponding to the wavelengths 425 nm (violet), 525 nm (green), 600 nm (orange), and 770 nm (transition to infrared). The presence of these spectral signatures indicates the selective absorption of visible light due to the insertion of Cr^{3+} chromophore ions into the crystal lattice of β-$LiAlSi_2O_6$. For the wavelengths analyzed in the near-infrared range, no relevant signatures were identified. This region of the spectrum is responsible for absorptions associated with high-energy functional groups, which, because they involve atoms of relatively low mass, have harmonic transitions in this region of the spectrum[38].

The occurrence of selective absorption by the material is produced by the introduction of chromophore ions of Cr^{3+} in the structure of β-$LiAlSi_2O_6$, which, when interacting with

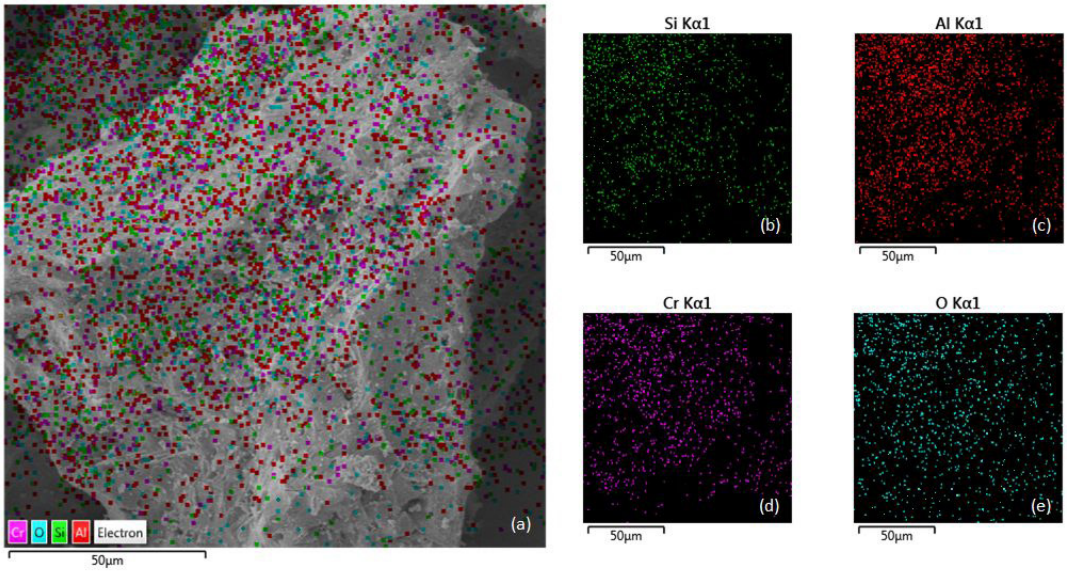

Figure 3. SEM image and overlaid EDS of β-$LiAlSi_2O_6$:3%Cr sample. The micrograph has a magnification of 1000x.

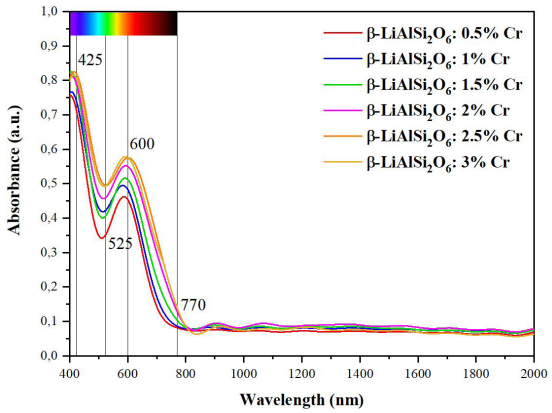

Figure 4. Vis-NIR absorption spectra of β-$LiAlSi_2O_6$:Cr samples.

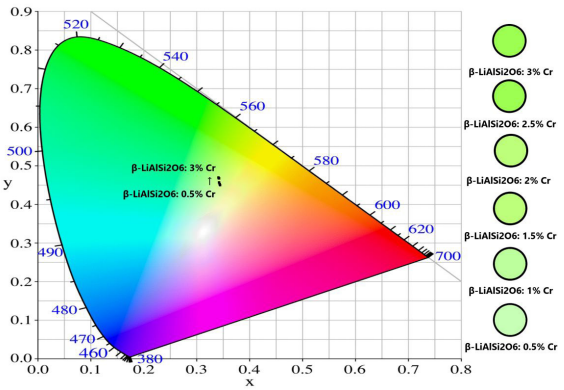

Figure 5. CIE-XYZ (1931) diagram chromatic coordinates of β-$LiAlSi_2O_6$:Cr samples. The coordinates were generated from the radiance emitted by the halogen light used by the vis-NIR DRS, and there may be variations in the pigment color perception depending on the local luminosity.

visible radiation, are responsible for promoting electronic transitions from the valence band to the conduction band. The color of Cr^{3+}-doped materials is explained by the crystal field theory, and this dopant has a d^3 electronic configuration and in oxides presents octahedral coordination[39]. The two absorption bands that occur in the visible region (425 nm and 600 nm) are attributed to the transitions $^4A_{2g} \rightarrow {}^4T_{2g}(^4F)$ and $^4A_{2g} \rightarrow {}^4T_{1g}(^4F)$. Selective absorption occurs at higher relative intensities for the wavelengths of violet and orange light, and these optical absorption bands are responsible for identifying the pigment in the complementary yellowish-green color.

The spectra obtained demonstrate a tendency for an increase in the intensity of absorption in the visible light wavelength range as the Cr^{3+} content increases. This upward trend decreases for the β-$LiAlSi_2O_6$:3%Cr sample, demonstrating a possible saturation point, where the increase in the dopant concentration no longer exerts considerable variation in absorbance. Furthermore, the increase in the dopant content influences a slight increase in luminance (Y), when the color is characterized in terms of the chromaticity coordinates of the CIE-XYZ space, which is shown in Figure 5. All the coordinates for the samples produced are detailed in Table 2.

Just as the absorbance intensity tends to saturate, the luminance (Y) tends to stop growing, having a slight decrease for the β-$LiAlSi_2O_6$:3%Cr sample. Despite the increase in color intensity, the X coordinate, referring to the chromaticity plane, tends to remain constant with increasing Cr^{3+}. The colors obtained reveal a great potential for obtaining β-$LiAlSi_2O_6$:Cr-based pigment, which is monochromatic and can be produced with different intensities of yellowish-green. It is important to emphasize that possible changes in the crystal structure of β-$LiAlSi_2O_6$ can occur for Cr^{3+}

Table 2. CIE-XYZ (1931) colorimetric coordinates for β-$LiAlSi_2O_6$:Cr samples.

Sample	X	Y	Z
β-$LiAlSi_2O_6$:0.5%Cr	0,3561	0,3847	0,2592
β-$LiAlSi_2O_6$:1%Cr	0,3554	0,3873	0,2574
β-$LiAlSi_2O_6$:1.5%Cr	0,3544	0,3916	0,2539
β-$LiAlSi_2O_6$:2%Cr	0,3543	0,4019	0,2428
β-$LiAlSi_2O_6$:2.5%Cr	0,3533	0,4038	0,2429
β-$LiAlSi_2O_6$:3%Cr	0,3539	0,4016	0,2445

contents over 3%, as already demonstrated in the Rietveld refinement (Figure 2). As an absorbance saturation point was observed for the β-$LiAlSi_2O_6$:3%Cr sample (Figure 4), it is recommended to use up to 2.5% by weight percentage dopant to produce these pigments.

The β-$LiAlSi_2O_6$:Cr-based pigment has a great potential for application in materials of ceramic industry, and its performance can be evaluated on glass, plaster, porcelain, paints, among others. Although the β-$LiAlSi_2O_6$ matrix is thermally stable and chemically inert, and the addition of the Cr^{3+} dopant has not caused changes in this matrix or the formation of a second phase, no study on its toxicity has been conducted, and its use is recommended only in industrial applications. Its inhalation or ingestion, as well as any biotechnological application must be avoided.

4. Conclusions

The present work reports the development of a novel ceramic pigment, based on β-$LiAlSi_2O_6$ structure, a stable and chemically inert material, using the Cr^{3+}-doping process. A partial proteic sol-gel method was provided, using gelatin as a ligand, as an alternative to traditional methods that demand high synthesis temperatures. The results confirmed the viability of β-$LiAlSi_2O_6$ synthesis by this route and the possibility of doping this ceramic with Cr^{3+} ions to obtain a yellowish-green pigment.

XRD analyzes confirmed the formation of the single-crystal structure of β-$LiAlSi_2O_6$, and the Rietveld refinement indicated the absence of significant distortions in the lattice with doping up to 3.0% of Cr^{3+}. SEM image and overlaid EDS confirmed the homogeneous existence of Cr^{3+} dopant in β-$LiAlSi_2O_6$ particles and verified the great possibility of Cr^{3+} occupying Al/Si sites in its matrix. The vis-NIR DRS spectra confirmed the selective absorption of radiation in the bands of 425 nm and 600 nm and the increase in these absorbance intensities, as in luminance intensities for CIE-XYZ coordinates, with the addition in the doping content up to 2.5% of Cr^{3+}. This β-$LiAlSi_2O_6$:Cr-based pigment is inert and chemically stable and can be evaluated for performance in diverse materials in the ceramic industry.

5. Acknowledgments

The authors are thankful to the Brazilian Research Support Agencies: Coordenação de Aperfeiçoamento de Pessoal de Nível Superior - Brasil (CAPES) and the Ministério da Ciência, Tecnologia, Inovações e Comunicações – MCTIC, Chamada Pública MCTI/FINEP/FNDCT 02/2016 (Ref. 0533/16).

6. References

1. Buxbaum G, Pfaff G, editors. Industrial Inorganic pigments. Weinheim: Wiley-VCH; 2005.
2. Maslennikova GN, Pishch IV, Radion EV. Current classification of ceramic silicate pigments. Glass Ceram. 2006;63:281-4.
3. Zaichuk AV, Amelina AA. Production of uvarovite ceramic pigments using granulated blast-furnace slag. Glass Ceram. 2017;74:99-103.
4. Alimzhanova ZI, Kadyrova DS, Yusupova MN. Ceramic pigments based on raw materials from Uzbekistan. Glass Ceram. 2013;70:441-3.
5. Liu M, Peng Z, Wang X, He Y, Huang S, Wan J, et al. The effect of high energy ball milling on the structure and properties of two greenish mineral pigments. Dyes Pigments. 2021;193:109494.
6. Przywecka K, Kowalczyk K, Grzmil B. Sequential co-precipitation as a convenient preparation method of anticorrosive hybrid calcium phosphate/calcium silicate powder pigments. Powder Technol. 2020;373:660-70.
7. Zhang A, Mu B, Wang X, Wen L, Wang A. Formation and coloring mechanism of typical aluminosilicate clay minerals for $CoAl_2O_4$ hybrid pigment preparation. Front Chem. 2018;125(6):1-11.
8. Barlog M, Pálková H, Bujdák J. Luminescence of a laser dye in organically-modified layered silicate pigments. Dyes Pigments. 2021;191:109380.
9. Corradini M, Ferri L, Pojana G. Spectroscopic characterization of commercial pigments for pictorial retouching. J Raman Spectrosc. 2020;52(1):35-58.
10. Lima HRBR, Nascimento DS, Souza SO. Production and characterization of spodumene dosimetric pellets by prepared by Pechini and proteic sol–gel route. Radiat Meas. 2014;71:122-6.
11. d'Amorim RAPO, Vasconcelos DAA, Barros VSM, Khoury HJ, Souza SO. Characterization of α-spodumene to OSL dosimetry. Radiat Phys Chem. 2014;95:141-4.
12. Guedes M, Ferro AC, Ferreira JMF. Nucleation and crystal growth in commercial LAS compositions. J Eur Ceram Soc. 2001;21(9):1187-94.
13. Shu K, Xu L, Wu H, Xu Y, Luo L, Yang J, et al. In-situ adsorption of mixed anionic/cationic collectors in a spodumene feldspar flotation system: implications for collector design. Langmoir. 2020;36:8086-99.
14. Guo H, Yu H, Zhou A, Lü M, Wang Q, Kuang G, et al. Kinetics of leaching lithium from α-spodumene in enhanced acid treatment using HF/H_2SO_4 as medium. Trans Nonferrous Met Soc China. 2019;29:407-15.
15. Rossi M, Dell'Aglio M, De Giacomo A, Gaudiuso R, Senesi GS, De Pascale O, et al. Multi-methodological investigation of kunzite, hiddenite, alexandrite, elbaite and topaz, based on laser-induced breakdown spectroscopy and conventional analytical

techniques for supporting mineralogical characterization. Phys Chem Miner. 2014;41:127-40.
16. Walker G, El Jaer A, Sherlock R, Glynn TJ, Czaja M, Mazurak Z. Luminescence spectroscopy of Cr^{3+} and Mn^{2+} in spodumene ($LiAlSi_2O_6$). J Lumin. 1997;72-74:278-80.
17. Sedel'nikova MB, Pogrebenkov BM, Liseenko NV, Gorbatenko VV. Nonstoichiometric reactions producing ceramic pigments. Glass Ceram. 2011;68:76-9.
18. Pechini MP. Method of preparing lead and alkaline earth titanates and niobates and coating method using the same to form a capacitor. USA patent 3.330.697, 1967.
19. Wang Q, Chang Q, Wang Y, Wang X, Zhou J. Ultrafine $CoAl_2O_4$ ceramic pigment prepared by Pechini-sacrificial agent method. Mater Lett. 2016;173:64-7.
20. Santos SF, Andrade MC, Sampaio JA, Luz AB, Ogasawara T. Thermal stydy of TiO_2-CeO_2 yellow ceramic pigment obtained by the Pechini method. J Therm Anal Calorim. 2007;87:743-6.
21. Buzinaro MAP, Ferreira NS, Cunha F, Macedo MA. Hopkinson effect, structural and magnetic properties of M-type Sm^{3+}-doped $SrFe_{12}O_{19}$ nanoparticles produced by a proteic sol-gel process. Ceram Int. 2016;42:5865-72.
22. Catauro M, Barrino F, Poggetto GD, Crescente G, Piccodella S, Pacifico S. New SiO_2/caffeic acid hybrid materials: synthesis, spectroscopic characterization, and bioactivity. Materials. 2020;13(2):394.
23. Brinker CJ, Scherrer GW. Sol-gel science: the physics and chemistry of sol-gel process. London: Academic Press; 1990.
24. Danks AE, Hall SR, Schnepp Z. The evolution of 'sol–gel' chemistry as a technique for materials synthesis. Mater Horiz. 2016;3(2):91-112.
25. Macedo MA. Manufacturing process of thin oxide layers using processed coconut water (in Portuguese). Brazil Patent 9804719-1, 1998.
26. Menezes AS, Remédios CMR, Sasaki JM, Silva LRD, Goes JC, Jardim PM, et al. Sintering of nanoparticles of α-Fe_2O_3 using gelatin. J Non-Cryst Solids. 2007;353:1091-4.
27. Silva RM, Raimundo RA, Fernandes WV, Torres SM, Silva VD, Grilo JPF, et al. Proteic sol-gel synthesis, structure and magnetic properties of Ni/NiO coreshell powders. Ceram Int. 2018;44(6):6152-6.
28. Schirieber R, Gareis H. Gelatine handbook: theory and industrial practice. Weinheim: Wiley-VCH; 2007.
29. Rietveld HM. A profile refinement method for nuclear and magnetic structures. J Appl Cryst. 1969;2:65-71.
30. Bleicher L, Sasaki JM, Oliveira C, Santos P. Development of a graphical interface for the Rietveld refinement program DBWS. J Appl Cryst. 2000;33:1189.
31. Commission Internationale de l'Éclairage. Commission internationale de l'Eclairage proceedings. Cambridge: Cambridge University Press; 1931.
32. Chi-Tang L, Peacor DR. The crystal structure of $LiAlSi_2O_6$-II ("β spodumene"). Z Kristallogr. 1968;126:46-65.
33. Young RA, Sakthivel A, Moss TS, Paiva-Santos CO. DBSW-9411: an upgrade of the DBWS programs for Rietveld refinement with PC and mainframe computers. J Appl Cryst. 1995;28(3):366-7.
34. Young RA, editor. The Rietveld method. New York: Oxford University Press; 1993.
35. Dinnebier RE, Leineweber A, Evans OSO. Rietveld refinement: practical powder diffraction pattern analysis using TOPAS. Berlin: de Gruyter; 2019.
36. David WIF. Powder diffraction: least-squares and beyond. J Res Natl Inst Stand Technol. 2004;109:107-23.
37. Barbosa LI, Valente G, Orosco RP, González JA. Lithium extraction from β -spodumene through chlorination with chlorine gas. Miner Eng. 2014;56:29-34.
38. Skoog DA, Holler J, Crouch SR. Principles of instrumental analysis. Boston: Cengage Learning; 2018.
39. Parlov RS, Marzá VB, Carda JB. Electronic absorption spectroscopy and colour of chromium-doped solids. J Mater Chem. 2002;12:2825-32.